

Synthesis and fabrication of ZnO–CuO doped PVA and ZnO–PbO doped PVA nanocomposite films by using γ -radiolysis and its microbial sensor application

H. Abdullah · Noor Azwen Noor Azmy ·
Norshafadzila Mohammad Naim · Aidil Abdul Hamid ·
Sarada Idris

Received: 14 June 2014 / Accepted: 29 October 2014 / Published online: 15 November 2014
© Springer Science+Business Media New York 2014

Abstract The fabricated of ZnO–CuO doped PVA and ZnO–PbO doped PVA nanocomposite thin films for determination of *Escherichia coli* has been investigated. ZnO–CuO doped PVA and ZnO–PbO doped PVA nanocomposite thin films were fabricated by sol–gel spin coating method and were exposed to ^{60}Co γ -radiation source at difference dose rate, between 0 and 30 kGy at room temperature. The resulting materials were investigated using X-ray diffraction, atomic force microscopy, transmission electron microscopy (TEM), field emission scanning electron microscopy (FESEM), UV–visible spectroscopy and current–voltage (I – V) measurement. The XRD spectra have been performed to observe the formation of crystal phases of all pure ZnO–CuO doped PVA and ZnO–PbO doped PVA thin films. The diffraction patterns reveal good crystalline quality. TEM and FESEM showed the uniform distribution of nanoparticles of metal oxides. Effect of γ -radiation on thin films decreased the crystallite size, surface morphology and grain size of thin films. UV–visible spectroscopy indicates the energy band gap, E_g decreased as the γ -radiation increased. The nanocomposite thin films prepared by γ -radiation can be applied to be used as biosensor materials.

Keywords PVA–ZnO–CuO · PVA–ZnO–PbO ·
Nanocomposite · Thin films · γ -Radiation · Biosensor

1 Introduction

Environmental monitoring for the detection of contaminated environment, such as chemical compounds, toxins and pathogens is essential to assess and avoid risks for both human and environmental wellness [1]. Biosensors constitute a good alternative for determination and identification of the microorganisms in contaminated food and water. Biosensors are defined by International Union of Pure and Applied Chemistry (IUPAC) as an integrated receptor-transducer devices that uses specific biochemical reactions mediated by isolated enzymes, immunosystems, tissues, organelles or whole cells to detect chemical compounds usually by electrical, thermal or optical signals [1, 2]. *Escherichia coli* (*E. coli*) are major causes of water and food-borne diseases in many countries [3, 4]. It can produce toxins that damage the inside layer of the intestine, causes anemia, stomach cramps and bloody diarrhea [5].

Nanomaterial metal oxides are transpired to have unique ability to promote more expeditious electron transfer kinetics between electrode and the active site of the desired enzyme [6]. On the other hand, nanomaterial metal oxides considered as most promising candidates because of their nontoxic nature, high thermal stability, photocatalytic and antibacterial properties [7]. Furthermore, nanomaterial metal oxides have been utilized in bioanalytical chemistry as a strategy to amend the analytical properties of the resulting sensor contrivances [8]. Among nanomaterial metal oxides, zinc oxide (ZnO) procured technological essential for biosensors, perspicacious windows and dye sensitized solar cells, etc. because of their properties

H. Abdullah (✉) · N. A. N. Azmy · N. M. Naim
Department of Electrical, Electronic and System Engineering,
Faculty of Engineering and Built Environment, UKM,
43650 Bangi, Selangor, Malaysia
e-mail: huda@vlsi.eng.ukm.my; huda@eng.ukm.my

A. A. Hamid
School of Biosciences and Biotechnology, Faculty of Science
and Technology, UKM, 43650 Bangi, Selangor, Malaysia

S. Idris
Radiation Facilities Division, Malaysian Nuclear Agency, Block
42, 43000 Bangi, Kajang, Selangor, Malaysia

including high surface area, catalytic efficiency, isoelectric point ~ 9.5 and vigorous adsorption ability [6]. It additionally demonstrates consequential magnification inhibition of a broad spectrum of bacteria [9].

There are various methods to make metal oxides thin films, but among the various methods, the sol–gel method is one of useful and attractive technique. Sol–gel derived bioactive platform was constructed for detection of pathogenic germs, *E. coli* [10]. The design flexibility of sol–gel method and the simplicity of fabrication can fulfil to create the surfaces with structural and chemical characteristics that could be compatible with biomaterials such as antibodies, enzymes, receptors, etc [10]. Moreover, the sol–gel method is simple to prepare and has several advantages such as, high purity, high homogeneity, low processing temperatures, low cost of fabrication, chemical inertness, physical rigidity, tuneable properties and negligible swelling in aqueous and non-aqueous solution [7, 11–13].

On the other hand, γ -radiation is used to alter, the morphological, optical and electrical properties of the thin film nanocomposites [14]. As reported by Alarcón et al., γ -radiation can give unique conditions to control the composition and morphology of ZnO particles for photocatalytic disinfection of contaminated water. Therefore, the efficiency of disinfection appears to be correlated with the texture of the film [15].

In this work, we have been exploring the synthesis between ZnO–CuO doped PVA and ZnO–PbO doped PVA nanocomposite films by γ -radiation. The sol–gel method was used to prepare ZnO–CuO doped PVA and ZnO–PbO doped PVA nanocomposite films. The nanocomposite films have been characterized for the study of several physical properties such as structural, morphological and optical properties. Furthermore, the nanocomposite thin films for microbial sensor were fabricated and its sensitivity was measured.

2 Methodology

2.1 Sample preparations

The precursors zinc acetate dehydrates [$\text{Zn}(\text{CH}_3\text{CO}_2)_2 \cdot 2\text{H}_2\text{O}$] and copper acetate [$\text{Cu}(\text{CH}_3\text{COO})_2$] were dissolved in ethanol and added to the PVA solution in distilled water. Apart from that, the precursors zinc acetate dehydrates [$\text{Zn}(\text{CH}_3\text{CO}_2)_2 \cdot 2\text{H}_2\text{O}$] and lead (IV) acetate [$\text{Pb}(\text{C}_2\text{H}_3\text{O}_2)_4$] also were dissolved in ethanol and added to the PVA solution in distilled water. All solutions were mixed at $60^\circ\text{C}/24\text{ h}$ using magnetic stirred until a gel formation, clear and stable solution is obtained. The glass substrates were first cleaned in methanol and acetone. Then the substrates were rinsed with deionized water. The substrates were rotated at a speed 4,000 rpm for 30 s using spin coater. Then, the coated

substrates were heated at or 10 min after each coating. By repeating the above procedure five times, five layers of coatings were obtained. Having completed the five layers of coatings, the thin film samples were annealed at 450°C for 1 h in a furnace to achieve the crystal phase. Then, the thin films were irradiated by ^{60}Co γ -irradiator at Malaysian Nuclear Agency. The metal oxides were exposed to ^{60}Co γ -radiation source at difference dose rate, ranging from 0 and 30 kGy at room temperature.

2.2 Characterizations

The orientations of the thin film samples were determined by X-ray diffraction measurements (XRD) with Cu $K\alpha$ irradiation ($\lambda = 1.5406\text{ \AA}$) and Bragg angle, 2θ ranged from 20° to 60° . Structural properties of the produced samples were analyzed using atomic force microscopy, (AFM), transmission electron microscopy (TEM) and field emission scanning electron microscopy (FESEM) to determine the morphology of the thin films. The optical characterization of samples was carried out using Perkin Elmer UV–visible spectroscopy.

2.3 Bacteria culture conditions and fabrication of microbial sensors

The bacterial strains used in this study originate from the bacterial collection of School of Biosciences and Biotechnology, UKM. *E. coli* was selected as a gram-negative bacterial model. The bacterial colonies were first grown on sterile solid nutrient agar medium. From primary cultured agar plates, fresh colonies were inoculated into 250 mL nutrient broth medium and grown overnight. The concentration of *E. coli* in the stock solution was 10^8 colony forming units (CFU/mL) determine by the number of viable cells. The glass substrates with metal oxides films were cut into $19\text{ mm} \times 25\text{ mm} \times 1\text{ mm}$ piece. A comb-type structure of silver electrode was sputtered on the nanocomposite thin films for $1,000\text{ \AA}$ thickness. Copper wires were soldered to the silver electrodes as the connection between thin film and the measuring instrument. The sensor performance was conducted using GAMRY Physical Electrochemistry by measuring I–V characteristics of the thin film. This preparation procedure was summarized in flowchart as shown in Fig. 1.

3 Result and discussion

3.1 Structural studies (XRD)

XRD patterns of radiated and un-radiated ZnO–CuO doped PVA and ZnO–PbO doped PVA samples are given in

Fig. 1 Flowchart for sample preparation procedure for ZnO–CuO doped PVA and ZnO–PbO doped PVA nanocomposite films by γ -radiation

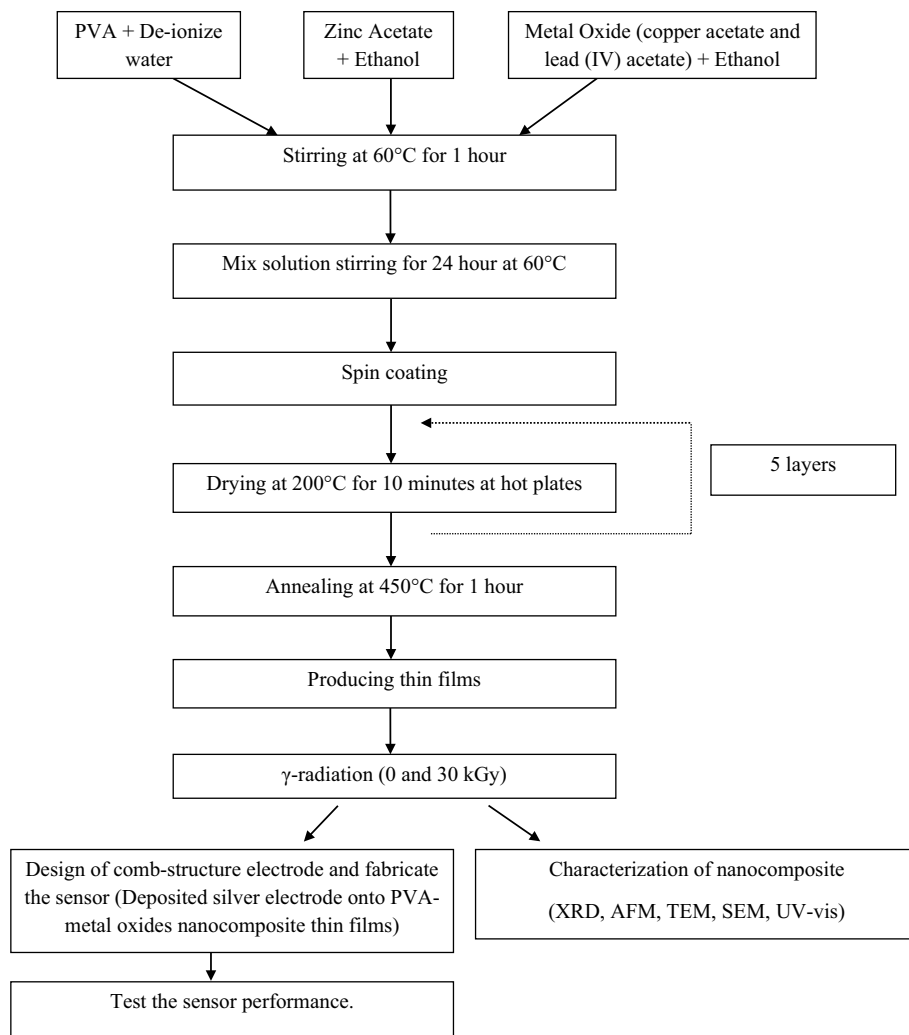
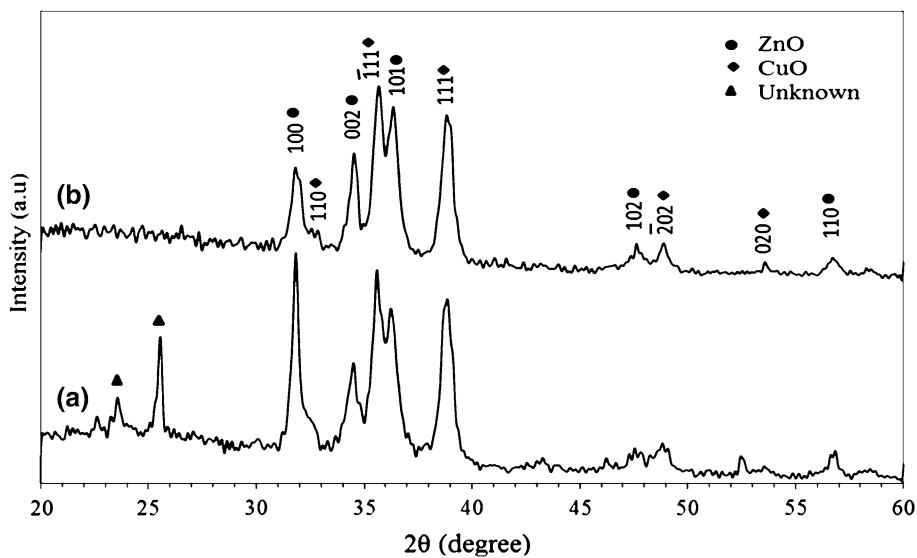


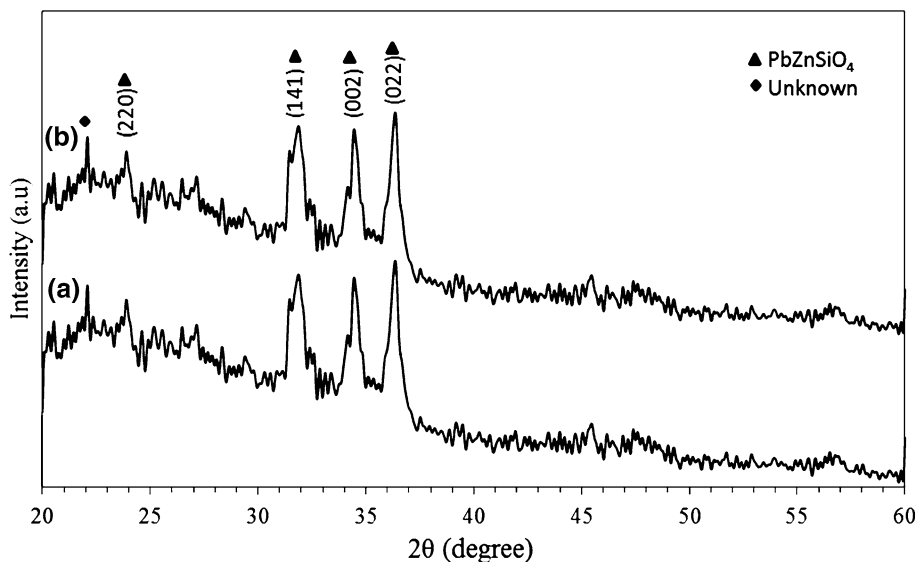
Fig. 2 XRD pattern of ZnO–CuO doped PVA thin films fabricated from γ -radiation precursor at (a) 0 kGy, (b) 30 kGy



Figs. 2 and 3, respectively. XRD analysis was used to extend the crystallization of the samples [13]. In the XRD spectra of ZnO–CuO doped PVA nanoparticles, we can

observe the formation of well crystalline and the indexed peaks in these XRD patterns are fully fitted with the corresponding hexagonal structure ZnO (Zincite syn, JCPDS

Fig. 3 XRD pattern of ZnO–PbO doped PVA thin films fabricated from γ -radiation precursor at (a) 0 kGy, (b) 30 kGy



01-070-8070) and monoclinic structure CuO (Tenorite syn, JCPDS 01-073-6023). The dominant peak (101) of pure ZnO and (111) of pure CuO was selected as preferential orientation along c-axis. On the other hand, ZnO–PbO doped PVA corresponded to the standard pattern of orthorhombic PbZnSiO₄ (Larsenite syn, JCPDS 00-020-0607) with the dominant peak (141).

Figure 2 shows the major diffraction peaks for pure ZnO has been observed at $2\theta = 31.9^\circ, 34.5^\circ, 36.3^\circ, 47.5^\circ$ and 56.9° corresponding to (100), (002), (101), (102), and (110) diffractions of ZnO, respectively. The pure CuO film reveals peaks at $2\theta = 32.1^\circ, 35.6^\circ, 38.9^\circ, 48.8^\circ$ and 53.6° corresponding to (110), ($\bar{1}11$), (111), ($\bar{2}02$) and (020) diffractions of CuO, respectively. The observed diffraction peaks of ZnO and CuO are consistent with those reported by Caglar et al. [16] and Habibi et al. [17]. From Fig. 2 one may conclude that the ZnO and CuO component in the patterns have no obvious change, but the relative intensity of diffraction peaks has obvious change and that the peaks do not affect each other's position [18].

PbZnSiO₄ peaks in Fig. 3 appeared at $2\theta = 23.9^\circ, 31.8^\circ, 34.4^\circ$ and 36.3° corresponding to (220), (141), (002) and (022), respectively. These observations confirm that with increasing γ -radiation, the basic crystal structure remains the same, although a slight change in intensity is observed.

The crystallite sizes or grain sizes of the thin film samples were calculated using Debye–Scherrer's equation [19, 20],

$$D = \frac{0.94\lambda}{\beta \cos \theta} \quad (1)$$

where, D is the crystallite size, λ is X-ray wavelength (1.5406 Å), β is full width at half maximum (FWHM) of the observed peak and θ is the diffraction angle. The

Table 1 Crystal size of ZnO–CuO doped PVA and ZnO–PbO doped PVA thin films fabricated from γ -radiation precursor

Film	γ -Radiation (kGy)	(hkl)	Crystallite size, D (nm)
ZnO–CuO doped PVA	0	ZnO 101	39.72
		CuO 111	30.26
	30	ZnO 101	31.78
		CuO 111	18.67
ZnO–PbO doped PVA	0	141	35.31
	30	141	21.18

average crystallite size was calculated by resolving the highest intensity peak. The average crystallite size of each component of radiated and un-radiated ZnO–CuO doped PVA and ZnO–PbO doped PVA samples were calculated within the range of 20° – 60° (2θ) from the broadening of XRD diffraction lines as being listed in Table 1. Table 1 show the disorder phenomena of crystallite size when γ -radiation increase. The crystallite size of the films became smaller with increasing γ -radiation indicating that the film crystallinity deteriorated [21]. As reported by Raneesh et al. [22], the γ -radiation can produced the compressive strain and also generated some disorder in the lattice structure.

3.2 Morphological observations

The atomic force microscopy (AFM) images of three-dimensional radiated and un-radiated ZnO–CuO doped PVA and ZnO–PbO doped PVA measured at room temperature are shown in Fig. 4. The scanning size was $1 \mu\text{m} \times 1 \mu\text{m}$. The AFM was used to analyze the topography of the surface. The surface roughness data on sample

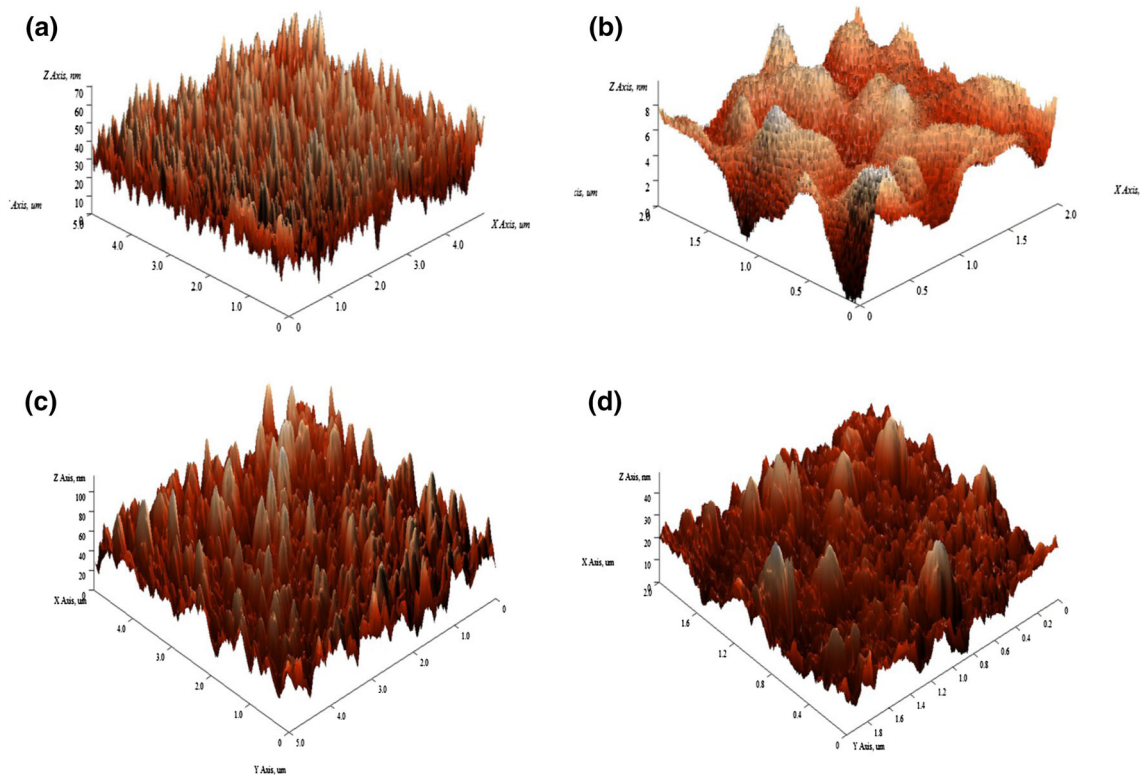


Fig. 4 AFM images of ZnO–CuO doped PVA and ZnO–PbO doped PVA thin films fabricated from γ -radiation precursor at **a** 0 kGy, **b** 30 kGy, **c** 0 kGy, **d** 30 kGy, respectively

Table 2 Surface roughness data on thin films at difference dose rate

Sample	γ -Radiation (kGy)	Roughness (nm)
ZnO–CuO doped PVA	0	7.281
	30	1.047
ZnO–PbO doped PVA	0	14.124
	30	4.728

thin films at different dose rate are given in Table 2. The radiated samples (Fig. 4b, d) had smoother surface areas compared with un-radiated (Fig. 4a, c) because of decreased grain and crystallite sizes. The textures are split into smaller grains due to the absorbed dose at 30 kGy. Furthermore, the grains of metal oxides thin film started to occur together and pile up at various spots on the surface of the film [21].

The size and the shape of metal oxides were investigated by transmission electron microscopy. The radiated ZnO–CuO doped PVA and ZnO–PbO doped PVA were shown in Figs. 5 and 6, respectively. From Fig. 5 shows the TEM images of radiated ZnO–CuO doped PVA which is homogeneous and agglomerated with a particle size ranging from 12.3 to 18.8 nm with an average diameter of ~ 15.6 nm. TEM images of radiated ZnO–PbO doped PVA as shown in Fig. 6. The nanoparticles are homogeneous

with an average diameter of ~ 19.5 nm. From our observation, the thin film samples show agreement with the results of the crystallite size calculated from the peak broadening as shown in Table 1.

Surface morphological studies of the film samples also were carried out using FESEM. Figure 7a, b shows the FESEM images of un-radiated and radiated ZnO–CuO doped PVA, respectively. The surface of the deposited films is very smooth and well packed with quasi-spherical grains and peanut shaped particles. In order to eliminate the pore structure, the γ -radiation dosed needs to be increase as this process will produce more compact and homogeneous structure of the samples. The decreasing of the crystallite sizes with the increase γ -radiation dosed was in agreement with the reduction of the thin film particle sized observed by the FESEM images. In fact, the particles are derived from the agglomeration or aggregation of many small crystals.

3.3 Optical band gap

The absorption spectra of ZnO–CuO doped PVA and ZnO–PbO doped PVA nanoparticles with radiated and un-radiated are measured in the wavelength range of 300 nm–800 nm. The energy band gap (E_g) can be determined by plotting the curve of $(\alpha h\nu)^2$ against the photon energy, $h\nu$,

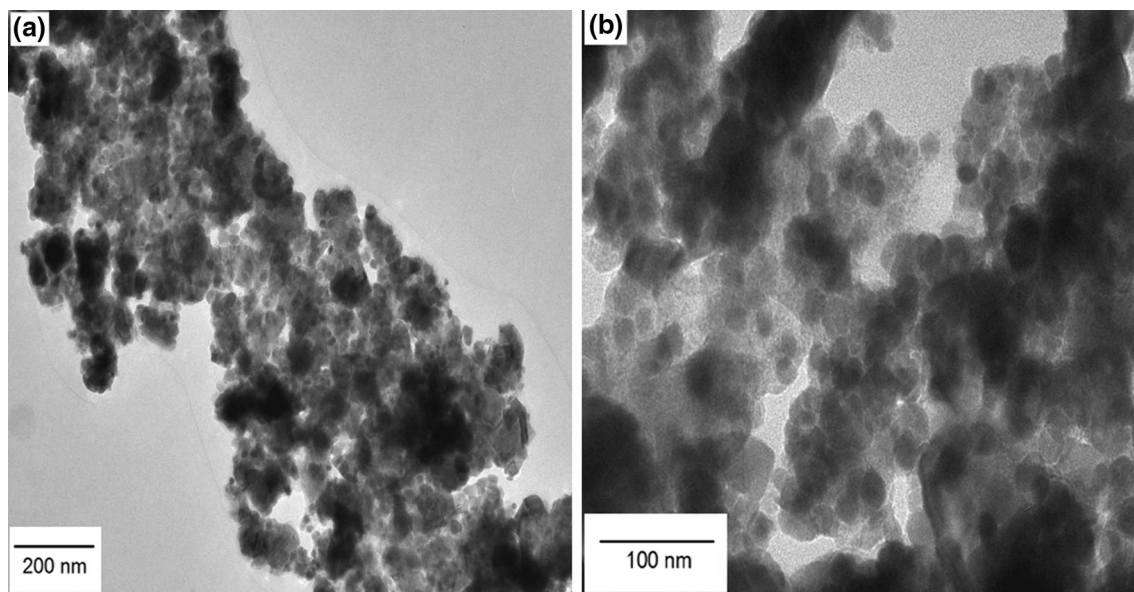


Fig. 5 TEM images of radiated ZnO–CuO doped PVA

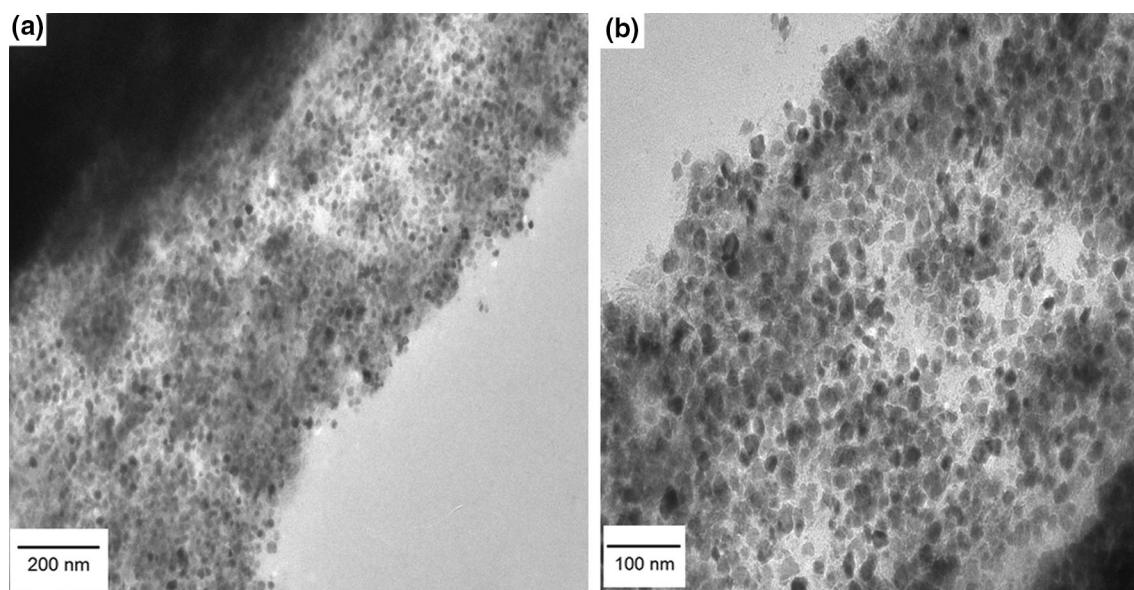


Fig. 6 TEM images of radiated ZnO–PbO doped PVA

and extrapolating the linear portion of the curve to the $h\omega$ axis. The E_g for the films can be calculated using Tauc's equation [20, 23–25],

$$\alpha h\omega = \text{const}(h\omega - E_g)^n \quad (2)$$

and $n = 1/2$ for direct transition. This relation holds very well above the exponential tail, where it presents a linear behavior. The graph of $(\alpha h\omega)^2$ versus $h\omega$ for sample nanocomposite thin films are shown in Fig. 8. From these spectra, the band gap energy obtained for un-radiated ZnO–CuO doped PVA and ZnO–PbO doped PVA is (a) $E_g = 3.80$ eV and

(c) $E_g = 3.30$ eV whereas the for radiated ZnO–CuO doped PVA and ZnO–PbO doped PVA, containing 30 kGy have (b) $E_g = 2.70$ eV and (d) $E_g = 2.90$ eV respectively which is slightly attributed to other reported by Baydogan et al. [21]. From Fig. 8, it can clearly be seen that the band gap energies of the ZnO materials show decrease with the increase of γ -radiation. This decrease in the optical band gap basically due to the increase in the energy width of the band tails of localized states, similar observations have also been reported by other researcher [26–28]. As report by Sharma et al. [29], irradiation with γ -rays are assumed to create displacements of ions or

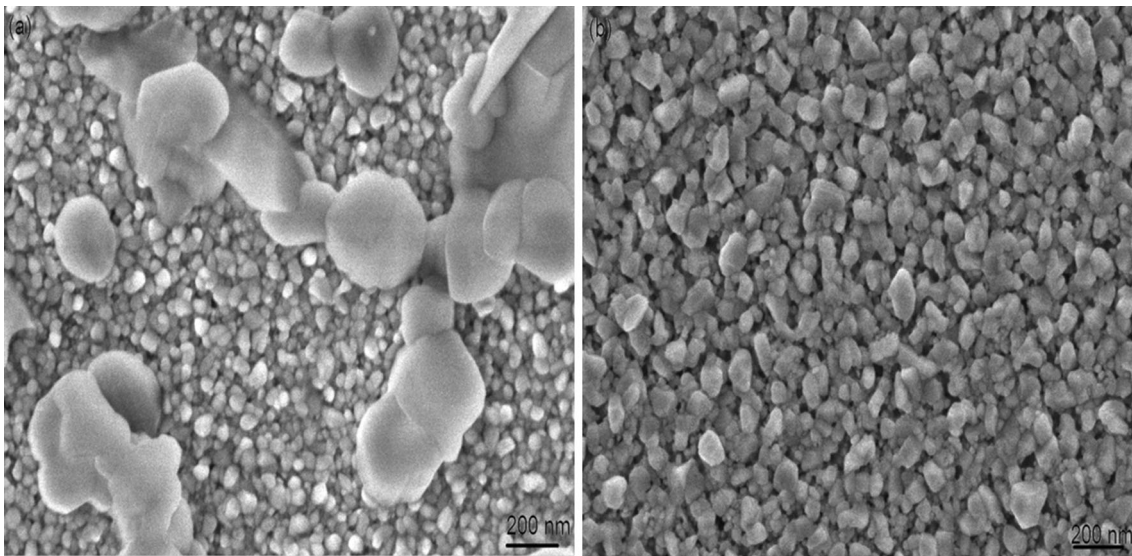


Fig. 7 FESEM images of **a** un-radiated sample and **b** radiated sample (30 kGy) ZnO–CuO doped PVA film

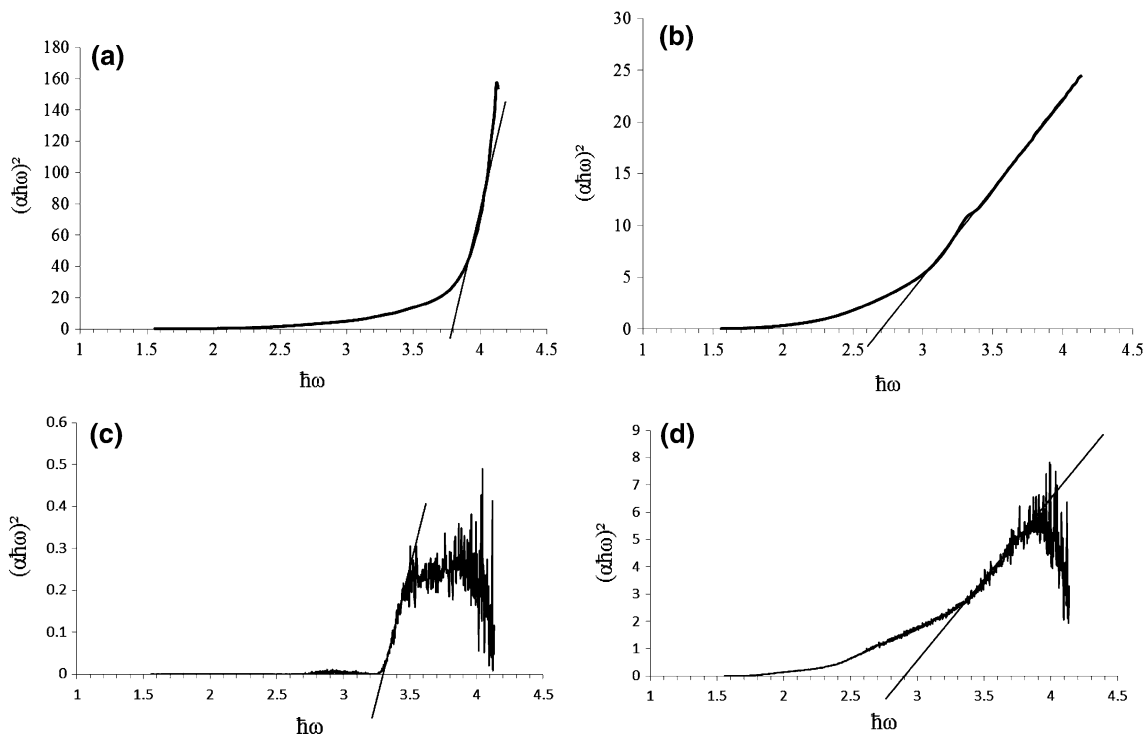


Fig. 8 The optical band gap of ZnO–CuO doped PVA and ZnO–PbO doped PVA thin films fabricated from γ -radiation precursor at **a** 0 kGy, **b** 30 kGy, **c** 0 kGy, **d** 30 kGy, respectively

breakage of bonds, allowing the structure to relax and fill the relatively large interstices that exist in the network of atoms.

3.4 Detection of *E. coli* bacteria by I–V measurement

The metal oxides nanocomposite synthesized onto a glass substrate was used for the detection of *E. coli* bacteria in

water. The Gram negative bacteria *E. coli* are selected in the current study since it is well-studied model organisms for antibacterial experiments [30]. The microbial sensor activities of metal oxides thin films were analyzed utilizing the principle of interaction of electrical charges on the microbe’s cell wall with the dangling bonds of metal oxides, particularly in thin films [31]. The sensing study of

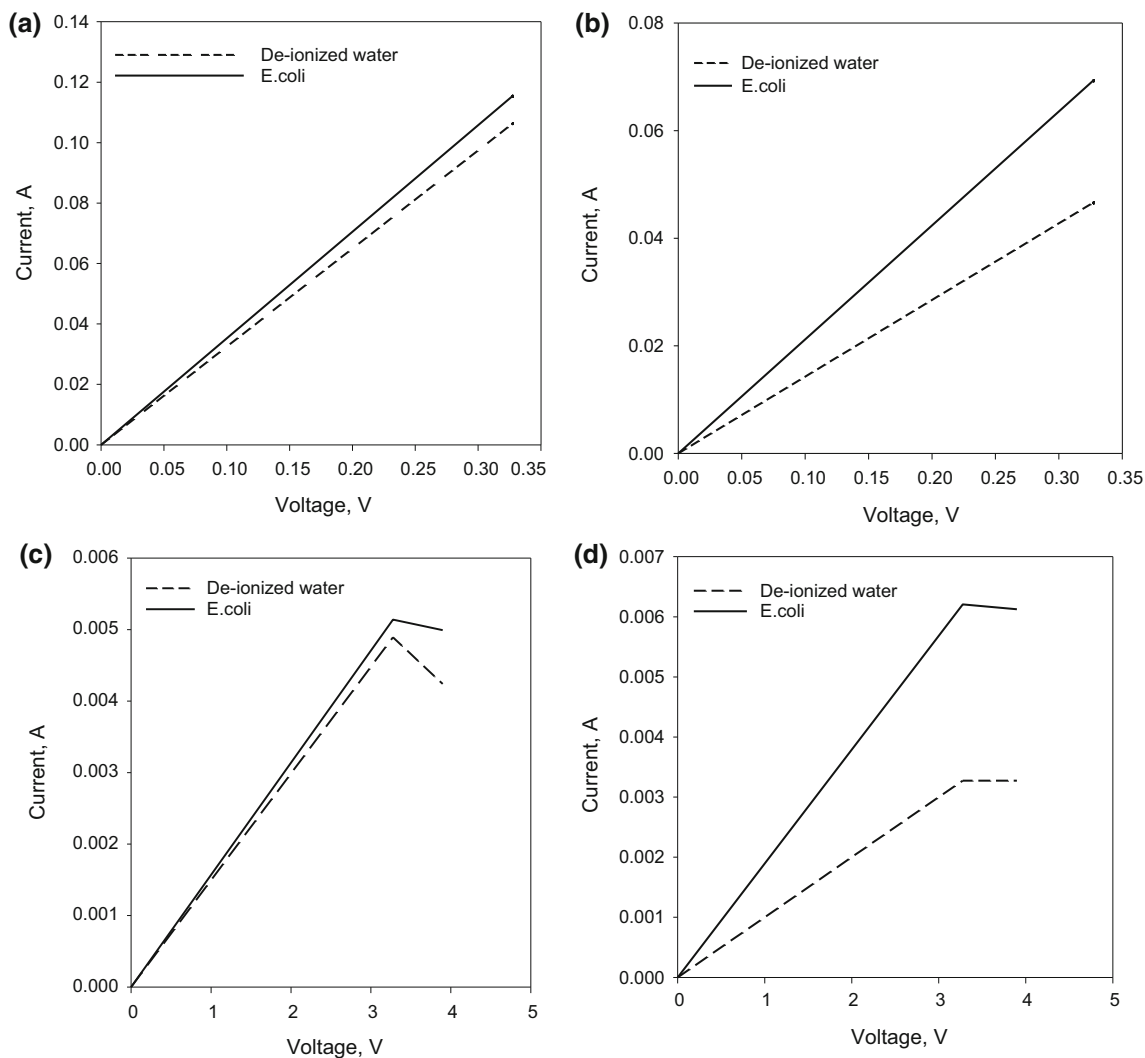


Fig. 9 Current–voltage measurement of ZnO–CuO doped PVA and ZnO–PbO doped PVA thin films fabricated from γ -radiation precursor at **a** 0 kGy, **b** 30 kGy, **c** 0 kGy, **d** 30 kGy, respectively

ZnO–CuO doped PVA and ZnO–PbO doped PVA nanoparticles with radiated and un-radiated were measured with and without exposure to *E. coli* at room temperatures as shown in Fig. 9. The outcome shows a rise in output current from the sensor as it is exposed to the *E. coli*; as can be seen, the positive charged of Zn^{2+} , Cu^{2+} and Pb^{4+} could be attached to the negative charged *E. coli* [32]. According to Matai et al. [33] and Abdullah et al. [34], ZnO nanocomposite may interact directly with the bacterial cell membrane by release Zn^{2+} upon surface oxidation or via porosity of composite or by electrostatic interactions between the ions released and the negatively charged bacterial cell wall. From the results shown in Fig. 9 also can be seen the influence of γ -radiation and the sensibility of the sensor observed to be higher with increasing γ -radiation. According to Azmy et al. [32], vegetative cells of

bacteria also are known to be really sensitive to gamma radiation.

4 Conclusion

ZnO–CuO doped PVA and ZnO–PbO doped PVA nanocomposite thin films for determination of *E. coli*, radiated and un-radiated, were successfully deposited on glass substrates and synthesized through the sol–gel method. After γ -radiation, the films depict very good structure, morphology, optical and electrical properties. X-ray diffraction analysis shows the presence of peak in the concentration and the present of peak indicates high crystallinity. Increasing the γ -radiation dose decreased the crystallite size, grain size, surface morphology and energy

band gap, E_g of the films. The presence of *E. coli* in the water was identified by measuring the changes of conductivity of thin film using I – V measurement and it proposed to be higher at a higher radiation dose.

Acknowledgments This project was supported by an Exploratory Research Grants Scheme (ERGS/1/2012/STG05/UKM/02/5), Islamic Educational, Scientific and Cultural Organization (ISESCO) (KK-2013-006), Photonic Technology Laboratory, Department of Electrical, Electronic and System Engineering, Universiti Kebangsaan Malaysia, Bangi, Selangor, Malaysia, School of Biosciences and Biotechnology, Faculty of Science and Technology, 43650 UKM, Bangi, Selangor, Malaysia and MINTect—SINAGAMA, Malaysia Nuclear Agency, Bangi, Selangor, Malaysia.

References

1. Van Dorst B, Mehtaa J, Bekaert K, Rouah-Martin E, De Coen W, Dubruel P, Blust R, Robbens J (2010) Biosens Bioelectron 26:1178–1194
2. Nayak M, Kotian A, Marathe S, Chakravorty D (2009) Biosens Bioelectron 25:661–667
3. Kandpal M, Gundampati RK, Debnath M (2009) World Academy of Science, Engineering and Technology, p 58
4. Kundu D, Gill A, Lui C, Goswami N, Holley R (2014) Meat Sci 96:413–418
5. Chowdhury AD, De A, Chaudhuri CR, Bandyopadhyay K, Sen P (2012) Sens Actuators B 171–172:916–923
6. Das M, Sumana G, Nagarajan R, Malhotra BD (2009) Thin Solid Films 519:1196–1201
7. Jan T, Iqbal J, Ismail M, Badshah N, Mansoor Q, Arshad A, Ahkam QM (2014) Mater Sci Semicond Process 21:154–160
8. Redondo-Marugan J, Petit-Dominguez MD, Casero E, Vázquez L, García T, Parra-Alfambra AM, Lorenzo E (2013) Sens Actuators B 182:307–314
9. Gordon T, Perlstein B, Houbara O, Felner I, Banin E, Margela S (2011) Colloids Surf A Physicochem Eng Asp 374:1–8
10. Lee W, Park K-S, Kim Y-W, Lee WH, Choi J-W (2005) Biosens Bioelectron 20:2292–2299
11. Jeon H-J, Yi S-C, Oh S-G (2003) Biomaterials 24:4921–4928
12. Wan Jalal WN, Abdullah H, Zulfakar MS, Bais B, Shaari S, Islam MT (2013) Trans Indian Ceram Soc 72(4):215–224
13. Abdullah H, Zulfakar MS, Wan Jalal WN, Islam MT, Shaari S (2013) J Sol-Gel Sci Technol. doi:10.1007/s10971-013-3202-7
14. Chahal RP, Mahendia S, Tomar AK, Kumar S (2012) J Alloys Compounds 538:212–219
15. Alarcón J, Ponce S, Paraguay-Delgado F, Rodríguez J (2011) J Colloid Interface Sci 364:49–55
16. Caglar Y, Oral DD, Caglar M, Ilıcan S, Thomas MA, Wu K, Sun Z, Cui J (2012) Thin Solid Films 520:6642–6647
17. Habibi MH, Karimi B, Zendehelel M, Habibi M (2013) Spectrochim Acta Part A Mol Biomol Spectrosc 116:374–380
18. Nalbant A, Ertek O, Okur I (2013) Mater Sci Eng B 178:368–374
19. Raoufi D, Raoufi T (2009) Appl Surf Sci 255:5812–5817
20. Thongsuriwong K, Amornpitoksuk P, Suwanboon S (2013) Adv Powder Technol 24:275–280
21. Baydogan N, Ozdemir O, Cimenoglu H (2013) Radiat Phys Chem 89:20–27
22. Raneesh B, Saha A, Kalarikkal N (2013) Radiat Phys Chem 89:28–32
23. Smirnov M, Baban C, Rusu GI (2010) Appl Surf Sci 256:2405–2408
24. Chand P, Gaur A, Kumar A, Gaur UK (2014) Appl Surf Sci 307:280–286
25. Lupan O, Pauporté T, Chow L, Viana B, Pellé F, Ono LK, Cuenya BR, Heinrich H (2010) Appl Surf Sci 256:1895–1907
26. Abu El-Fadl A, El-Maghraby EM, Mohamad GA (2004) Cryst Res Technol 39(2):143–150
27. Al-Hamdani NA, Al-Alawy RD, Hassan SJ (2014) IOSR J Comput Eng 16(1):11–16
28. El Zawawi IK, Khalil NR, Mahdy MA (2012) J Mater Sci Mater Electron 23:520–527
29. Sharma G, Thind KS, Manupriya, Klare HS, Narang SB, Gerward L, Dangwal VK (2006) Nucl Instrum Methods Phys Res B 243:345–348
30. Panigrahi J, Behera D, Mohanty I, Subudhi U, Nayak BB, Acharya BS (2011) Appl Surf Sci 258:304–311
31. Dixit V, Tewari JC, Sharma BS (2006) Sens Actuators B 120:96–103
32. Azmy NAN, Abdullah H, Naim NM, Hamid AA, Shaari S, Mokhtar WHMW (2014) Radiat Phys Chem 103:108–113
33. Matai I, Sachdev A, Dubey P, Kumar SU, Bhushan B, Gopinath P (2014) Colloids Surf B Biointerf 115:359–367
34. Abdullah H, Naim NM, Azmy NAN, Hamid AA (2014) J Nanomater 2014:951640